Creating polarization singularities with an *N*-pinhole interferometer

Robert W. Schoonover
Department of Electrical and Computer Engineering, University of Illinois at Urbana-Champaign, 405 N. Mathews, Urbana, Illinois 61801, USA
and The Beckman Institute for Advanced Science and Technology, University of Illinois at Urbana-Champaign, 405 N. Mathews, Urbana, Illinois 61801, USA

Taco D. Visser
Department of Electrical Engineering, Delft University of Technology, Mekelweg 4, 2628 CD Delft, The Netherlands and Department of Physics and Astronomy, Free University, De Boelelaan 1081, 1081 HV Amsterdam, The Netherlands
(Received 26 January 2009; published 9 April 2009)

Recent studies of singularities in scalar wave fields in Young's classic experiment are extended to electromagnetic fields diffracted by an *N*-pinhole interferometer. Linearly polarized fields whose direction of polarization may be different at each pinhole are examined. It is shown that for two pinholes, only surfaces of linear polarization are created. For *N* larger than two, a rich structure of polarization singularities is found even when the location of the pinholes is arbitrary. In addition, there can be regions where the spectral density of the field is zero.

DOI: 10.1103/PhysRevA.79.043809 PACS number(s): 42.25.Fx, 42.25.Ja

I. INTRODUCTION

Singular optics [1,2] is a relatively new branch of physical optics that analyzes topological features in the vicinity of singular points in wave fields. Originally it dealt with *phase singularities* and *polarization singularities* in monochromatic fields [3–8]. Later it expanded to include spatially coherent, polychromatic fields in which *spectral anomalies* can occur [9]. More recently, *coherence singularities* in partially coherent fields have also been studied [10–15].

Several studies have been dedicated to identifying different kinds of field singularities that can occur in Young's interference experiment. Phase singularities and coherence singularities of the field resulting from the illumination of a multipinhole interferometer with a partially coherent field have been predicted [16–18] and observed [19,20]. Optical vortices produced in a three-pinhole experiment with monochromatic scalar fields have also been analyzed [21]. Furthermore, the evolution of different types of singularities in a two-slit configuration—phase singularities of monochromatic scalar fields, coherence singularities of partially coherent scalar fields, and polarization singularities of vector fields—has recently been described [22].

It is the aim of the present paper to elucidate the different types of polarization singularities that can occur in an *N*-pinhole experiment. Polarization singularities in monochromatic fields occur at positions (typically lines) where the polarization ellipse is circular and hence its orientation angle is undefined (*C* lines), and at positions (typically surfaces) where the ellipse has degenerated into a line and therefore its handedness is undefined (*L* surfaces) [1]. Often, these singular structures are examined in a specific plane, which leads to the identification of *C* points and *L* lines. We show that in the two-pinhole setup, with the field at each pinhole being linearly polarized, surfaces of linear polarization are created, but that circular polarization can only be created on, at most, a single surface. In the three-pinhole configuration, surfaces of linear polarization can be created, as can lines of circular polarization. These results are displayed only for planes perpendicular to the interferometer screen, resulting in lines and points rather than surfaces and lines. We show that for $N=3$ a rich polarization topology occurs even when the locations of the pinholes lack symmetry. The extension to an *N*-pinhole setup is also discussed, and field structures for $N=4$ and $N=7$ are presented for symmetric pinhole configurations.

Our analysis does not only shed light on Young's interference experiment, one of the seminal experiments in physics, but it can also be applied to spatial control of the state of polarization. Having this capability is essential in quantum optics [23], but also in classical optics [24] where many components and samples [25] are birefringent.

II. TWO-PINHOLE INTERFEROMETER

Consider an opaque screen occupying the plane $z=0$ that is perforated by two identical pinholes. The pinholes are located at

$$\mathbf{r}_1=(d,0,0), \quad \text{and} \quad \mathbf{r}_2=(-d,0,0). \tag{1}$$

The field incident upon the pinholes is taken to be monochromatic with frequency ω, and linearly polarized. It is also assumed that the field at each pinhole is of equal amplitude and co-phasal. Let us write the electric field at the *j*th pinhole as

$$\mathbf{E}_j(\omega)=E_0 e^{i\omega t}\hat{\mathbf{e}}_j, \quad (j=1,2), \tag{2}$$

where $E_0 \in \Re$, t denotes the time, and $\hat{\mathbf{e}}_j$ is a real unit vector that denotes the direction of polarization. The field at an observation point $\mathbf{r}=(x,y,z)$ then equals [26]

$$\mathbf{E}(\mathbf{r},\omega)=\bar{E}(\omega)\sum_{j=1}^{2}\frac{e^{ikR_j}}{R_j}\hat{\mathbf{e}}_j, \tag{3}$$

where $R_j=|\mathbf{r}-\mathbf{r}_j|$, $\bar{E}(\omega)=-iE_0 d\mathcal{A}\exp(i\omega t)/\lambda$, $d\mathcal{A}$ is the area of each pinhole, and $k=\omega/c=2\pi/\lambda$ is the wave number as-

sociated with frequency ω, with c being the speed of light in vacuum. Obviously, if $\hat{\mathbf{e}}_1 \| \hat{\mathbf{e}}_2$, the resultant field will be linearly polarized everywhere. As is shown in the Appendix, all polarization choices except $\hat{\mathbf{e}}_1 \| \hat{\mathbf{e}}_2$ result in the same topological structure. We will therefore consider the case of two orthogonally polarized fields, namely, $\hat{\mathbf{e}}_1 = \hat{\mathbf{x}}$ and $\hat{\mathbf{e}}_2 = \hat{\mathbf{y}}$. Using this choice in Eq. (3), and by denoting

$$|E_x(\mathbf{r},\omega)| = E_0 d\mathcal{A}/\lambda R_1, \tag{4}$$

$$|E_y(\mathbf{r},\omega)| = E_0 d\mathcal{A}/\lambda R_2, \tag{5}$$

$$\delta = \arg[E_y(\mathbf{r},\omega)] - \arg[E_x(\mathbf{r},\omega)],$$

$$= k(R_2 - R_1), \tag{6}$$

the Stokes parameters that characterize the state of polarization of the field at position $\mathbf{r}$ can be expressed as [[26], Sec. 1.4.2]

$$S_0(\mathbf{r},\omega) = |E_x(\mathbf{r},\omega)|^2 + |E_y(\mathbf{r},\omega)|^2, \tag{7}$$

$$S_1(\mathbf{r},\omega) = |E_x(\mathbf{r},\omega)|^2 - |E_y(\mathbf{r},\omega)|^2, \tag{8}$$

$$S_2(\mathbf{r},\omega) = 2\,\mathrm{Re}\{E_x^*(\mathbf{r},\omega) E_y(\mathbf{r},\omega)\}, \tag{9}$$

$$S_3(\mathbf{r},\omega) = 2\,\mathrm{Im}\{E_x^*(\mathbf{r},\omega) E_y(\mathbf{r},\omega)\}. \tag{10}$$

The parameter $S_0(\mathbf{r},\omega)$ is proportional to the spectral density (or "intensity at frequency ω") of the field. The normalized Stokes vector (s_1, s_2, s_3) with $s_i = S_i/S_0$ and $i = 1,2,3$ indicates a point on the Poincaré sphere. The North Pole $(s_3 = 1)$ and South Pole $(s_3 = -1)$ both correspond to circular polarization. Points on the Equator $(s_3 = 0)$ correspond to linear polarization. All other points correspond to elliptical polarization. The orientation of the polarization ellipse also follows from the Stokes parameters.

Linear polarization occurs at positions where $s_3 = 0$. This implies that

$$\delta = k(R_2 - R_1) = n\pi, \tag{11}$$

with n an integer. Substitution of the definitions of R_1 and R_2 results in the equation

$$\frac{x^2}{a_n^2} - \frac{y^2}{b_n^2} - \frac{z^2}{b_n^2} = 1, \tag{12}$$

where

$$a_n^2 = n^2\lambda^2/16, \tag{13}$$

$$b_n^2 = d^2 - a_n^2 \quad (n = 1,2,\ldots,n_{\max}). \tag{14}$$

Since $|R_2 - R_1| < 2d$ it follows that

$$n_{\max} < 4d/\lambda \leq n_{\max} + 1, \tag{15}$$

and hence the coefficients b_n^2 are all positive. Equation (12) represents a set of $n_{\max}$ semihyperboloids of two sheets in the half-space $z > 0$, with their symmetry axis along the line connecting the two pinholes. The distance between the two x intercepts of each hyperbola equals $2a_n = n\lambda/2$. These intercepts all lie in between the two pinholes. An example of the first two hyperbolas $(n = 1,2)$ is shown in Figs. 1 and 2. Putting $n = 0$ in Eq. (11) yields an additional surface on which the field is linearly polarized, namely, the plane $x = 0$.

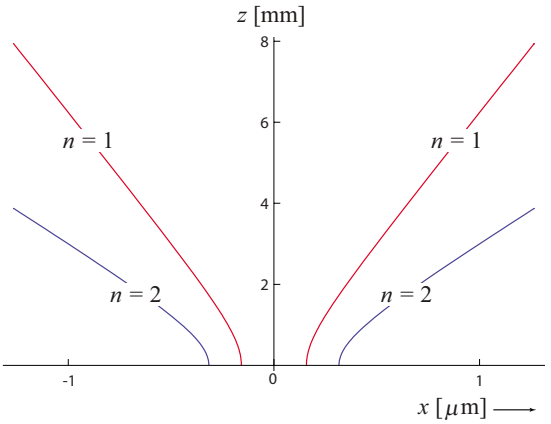

FIG. 1. (Color online) Semihyperbolas on which the polarization of the field in a two-pinhole interferometer is linear (L surfaces). In this example $\lambda = 632.8$ nm and $2d = 2$ mm. Notice that the horizontal scale is in microns, whereas the vertical scale is in millimeters.

Circular polarization occurs at positions where both $s_1 = 0$ and $s_2 = 0$. The first condition implies that $R_1 = R_2$, i.e., $x = 0$. From the second condition it follows that

$$\delta = k(R_2 - R_1) = (m + 1/2)\pi, \tag{16}$$

with m an integer. Substitution of the definitions of R_1 and R_2 results in the equation

$$\frac{x^2}{c_m^2} - \frac{y^2}{d_m^2} - \frac{z^2}{d_m^2} = 1, \tag{17}$$

where

$$c_m^2 = \left(m + \tfrac{1}{2}\right)^2 \lambda^2/16, \tag{18}$$

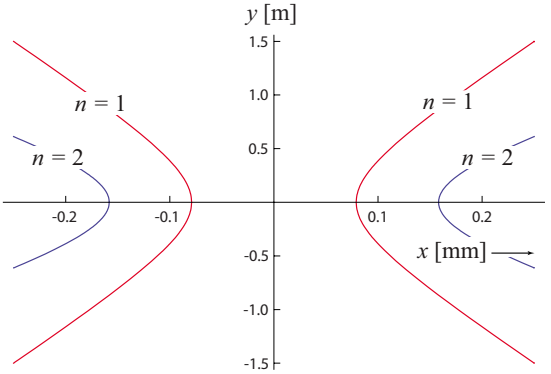

FIG. 2. (Color online) Semihyperbolas on which the polarization of the field in a two-pinhole interferometer is linear (L surfaces). In this example $z = 0.5$ m. All other parameters are as in Fig. 1. Notice that the horizontal scale is in millimeters, whereas the vertical scale is in meters.

$$d_m^2 = d^2 - c_m^2, \quad (m = 0, 1, \ldots, m_{\max}), \tag{19}$$

with

$$m_{\max} < \frac{4d}{\lambda} - \frac{1}{2} \leq m_{\max} + 1, \tag{20}$$

and the coefficients d_m^2 therefore all positive. Equation (17) represents a set of $m_{\max}+1$ semihyperboloids of two sheets in the half-space $z>0$, with their symmetry axis along the line connecting the two pinholes. The distance between the two x intercepts of each hyperbola equals $2c_m=(m+1/2)\lambda/2$. These intercepts too all lie in between the two pinholes. Since the surfaces of Eq. (17) and the plane $x=0$ do not intersect, the two conditions for circular polarization cannot be satisfied simultaneously and so there is no location at which the field is circularly polarized. It is shown in the Appendix that under less general conditions than discussed here, C points can occur in a $N=2$ configuration.

III. THREE-PINHOLE INTERFEROMETER

An example of a symmetric three-pinhole interferometer configuration is one in which the pinholes are located at the vertices of an equilateral triangle with sides $\sqrt{3}d$,

$$\mathbf{r}_1 = d(0,1,0), \quad \mathbf{r}_2 = d\left(\tfrac{-\sqrt{3}}{2}, \tfrac{-1}{2}, 0\right), \quad \mathbf{r}_3 = d\left(\tfrac{\sqrt{3}}{2}, \tfrac{-1}{2}, 0\right). \tag{21}$$

The field at each pinhole is taken to have amplitude E_0 and to be linearly polarized along the radial direction, i.e., $\hat{\mathbf{e}}_j=\hat{\mathbf{r}}_j$. This may be achieved, for example, by illuminating the screen with a radially polarized beam that propagates along the z axis [27]. In the region of superposition the field is given by

$$\mathbf{E}(\mathbf{r},\omega) = \bar{E}(\omega)\sum_{j=1}^{3} \frac{e^{ikR_j}}{R_j}\hat{\mathbf{e}}_j. \tag{22}$$

By inserting Eq. (22) into Eqs. (7)–(10), one may again analyze the Stokes parameters of the field in an observation plane. In Fig. 3, the color-coded spectral density is shown in the transverse plane $z=1$ m, with contours of $s_3=0$ (lines of linear polarization) superposed. A honeycomb pattern with many locations of near-zero spectral density is clearly visible. We also note that the line $x=y=0$ is a so-called V line, a line on which the total electric field is identically zero [1]. Both observations are a consequence of the particular choice of the pinhole positions. The appearance of a V line is reminiscent of the complete destructive interference of partially coherent scalar fields that has been predicted and observed for the same configuration [17,19,20].

There are three distinct sets of parallel L lines in the plane shown in Fig. 3. This structure may be understood as follows. If we apply the paraxial approximation

$$e^{ikR_j}/R_j \approx e^{ikr}e^{-ik\hat{\mathbf{r}}\cdot\mathbf{r}_j}/r, \tag{23}$$

where $r=|\mathbf{r}|$ in Eq. (22), then the Stokes parameter $S_3(\mathbf{r},\omega)$ is given by the expression

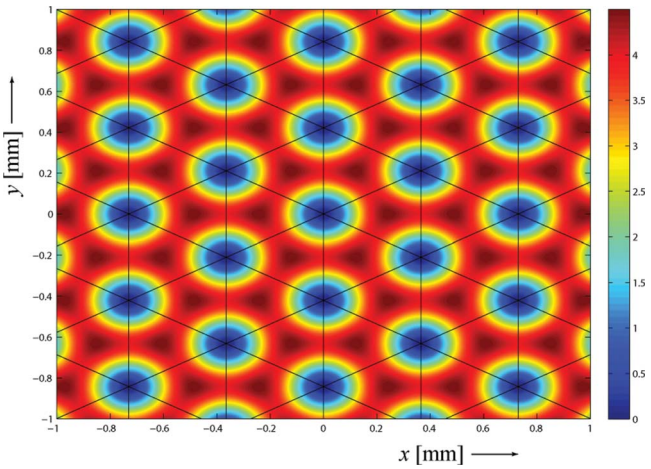

FIG. 3. (Color online) The spectral density (in arbitrary units) for the symmetric three-pinhole interferometer in the $z=1$ m plane. The solid black curves are lines of linear polarization. In this example $d=1$ mm and $\lambda=632.8$ nm.

$$S_3(\mathbf{r},\omega) = \frac{\sqrt{3}|\bar{E}(\omega)|^2}{r^2}\{\sin[k\hat{\mathbf{r}}\cdot(\mathbf{r}_1-\mathbf{r}_2)] + \sin[k\hat{\mathbf{r}}\cdot(\mathbf{r}_2-\mathbf{r}_3)] + \sin[k\hat{\mathbf{r}}\cdot(\mathbf{r}_3-\mathbf{r}_1)]\}. \tag{24}$$

By using the identity $\sin u+\sin v=2\cos[(u-v)/2]\sin[(u+v)/2]$ together with the relation $\mathbf{r}_1+\mathbf{r}_2+\mathbf{r}_3=0$, the first two terms on the right-hand side of Eq. (24) can be combined to give

$$S_3(\mathbf{r},\omega) = \frac{\sqrt{3}|\bar{E}(\omega)|^2}{r^2}\{-2\cos(3k\hat{\mathbf{r}}\cdot\mathbf{r}_2/2)\sin[k\hat{\mathbf{r}}\cdot(\mathbf{r}_3-\mathbf{r}_1)/2] + \sin[k\hat{\mathbf{r}}\cdot(\mathbf{r}_3-\mathbf{r}_1)]\}. \tag{25}$$

In this case, $S_3(\mathbf{r},\omega)$ vanishes when $k\hat{\mathbf{r}}\cdot(\mathbf{r}_3-\mathbf{r}_1)/2$ is a multiple of π. Any two of the three sine terms in Eq. (24) can be combined to simplify the equation, and the condition $S_3(\mathbf{r},\omega)=0$ can thus be generalized to

$$\hat{\mathbf{r}}\cdot(\mathbf{r}_i-\mathbf{r}_j) = p\lambda \quad (i,j=1,2,3 \quad \text{and} \quad i\neq j), \tag{26}$$

with p an integer. For each value of p this gives us three equations that approximate lines in a transverse observation plane $z=z_0$. Consider first the case $i=2$, $j=3$, for which $\mathbf{r}_i-\mathbf{r}_j=s\hat{\mathbf{x}}$, with $s=-\sqrt{3}d$. Inserting this into Eq. (26) yields the condition

$$x_p^2\left(1-\frac{p^2\lambda^2}{s^2}\right) = \frac{p^2\lambda^2}{s^2}(y_p^2+z_0^2), \tag{27}$$

where x_p and y_p are the locations of the pth L-line in the plane $z=z_0$. The number of L lines is bounded since $|p|\leq s/\lambda$. For $z_0=1$ m $\gg y_p$, and taking $d=1$ mm, $\lambda=0.6328$ μm, Eq. (27) reduces to

$$x_p \approx p\times 0.365 \text{ mm}, \tag{28}$$

the solutions of which correspond to the equidistant vertical L lines. On setting $i=1$, $j=3$ in Eq. (26), a similar derivation yields

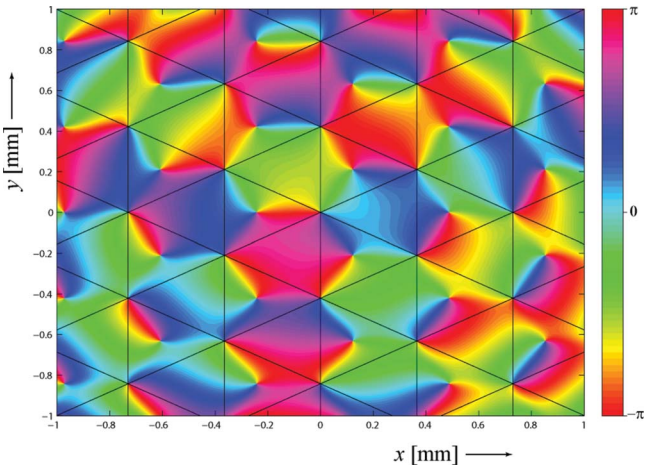

FIG. 4. (Color online) The phase of $E_+(\mathbf{r},\omega)$ in the $z=1$ m plane for the symmetric three-pinhole experiment. In this example $d=1$ mm and $\lambda=632.8$ nm. The phase singularities, points where all colors meet, correspond to C points, i.e., points of left-handed circular polarization.

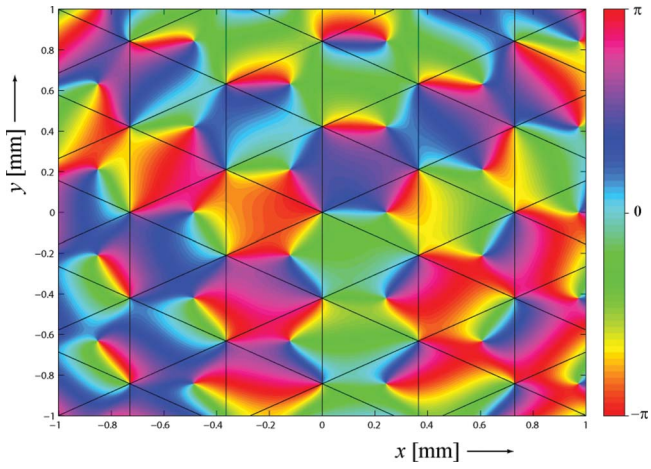

FIG. 5. (Color online) The phase of $E_-(\mathbf{r},\omega)$ in the $z=1$ m plane for the symmetric three-pinhole experiment. In this example $d=1$ mm and $\lambda=632.8$ nm. The phase singularities, points where all colors meet, correspond to C points, i.e., points of right-handed circular polarization.

$$y_0 \approx \frac{x_0}{\sqrt{3}} + p \times 0.422 \text{ mm}. \tag{29}$$

This expression describes the parallel L lines that run from the bottom left corner to the top right corner in Fig. 3. It is easily verified that by setting $i=1$, $j=2$ in Eq. (26) one obtains the approximation

$$y_0 \approx -\frac{x_0}{\sqrt{3}} + p \times 0.422 \text{ mm}, \tag{30}$$

which corresponds to the remaining set of L lines.

Unlike the two-pinhole case, circular polarization states do exist in the three-pinhole configuration. Right (left)-handed circular polarization may be thought of as the condition when the field amplitude in the left (right)-handed polarization basis state vanishes. The electric field amplitudes for any two orthogonal basis states are generally complex, and so the location of phase singularities of the right (left)-handed amplitudes correspond to states of complete left (right)-handed polarization. By decomposing the field as [[28], Sec. 7.2]

$$\mathbf{E}(\mathbf{r},\omega) = E_+(\mathbf{r},\omega)\hat{\mathbf{c}}_+ + E_-(\mathbf{r},\omega)\hat{\mathbf{c}}_-, \tag{31}$$

where

$$E_\pm(\mathbf{r},\omega) = \frac{E_x(\mathbf{r},\omega) \mp iE_y(\mathbf{r},\omega)}{\sqrt{2}}, \tag{32}$$

$$\hat{\mathbf{c}}_\pm = \frac{\hat{\mathbf{x}} \pm i\hat{\mathbf{y}}}{\sqrt{2}}, \tag{33}$$

the phase singularities of $E_+(\mathbf{r},\omega)$ and $E_-(\mathbf{r},\omega)$ may be found. In a color-coded plot of their phase, phase singularities are points where all colors meet. In Figs. 4 and 5, the phases are shown in the plane $z=1$ m. The location of the C points may be found approximately by again using Eq. (23) and solving for cases when $E_\pm=0$. These are points (x,y) in the plane $z=z_0$ that simultaneously satisfy the two conditions,

$$\frac{y}{z_0} = \frac{m\lambda}{3d}, \tag{34}$$

$$\frac{x}{z_0} = \frac{\beta_{mn}\lambda}{\pi\sqrt{3}d}, \tag{35}$$

where β_{mn} is the nth solution to $|\sqrt{3}\sin\beta_{mn}| = |1-(-1)^m\cos\beta_{mn}|$ and m and n are integers. Each m and n label a C point in the region of interest.

The condition for L lines and C points are trivially met by the case $\mathbf{E}=0$ (a V point). In fact, co-location of phase singularities for both E_+ and E_- is a necessary and sufficient condition for the existence of a V point. Likewise, a V point can be thought of as the intersection of an L line with a C point. Inspection of Figs. 4 and 5 shows many locations beyond $(x,y)=(0,0)$ that seem likely candidates for a V point. However, it follows from symmetry considerations that such a point can only occur on the z axis. Indeed it is found that the C points are all slightly off to the side of the L lines. The two types of singularities can only be shown to be co-located within the validity of the paraxial approximation—when $\sin\beta_{mn}=0$ in Eq. (35). The pairs of C points that are adjacent to the intersection of three L lines are of opposite topological charge—their phases circulate in opposite directions. This implies that half of them are "star"-type C points and the other half are either "lemon"- or "monstar"-type C points [29]. The C points that are not near an L-line intersection alternate between being stars and lemons along any of the three axes of symmetry. The C points closest to the intersections of multiple L lines are monstar-type polarization singularities. The distinction between monstars and lemons was made through inspection of plots of the orientation angles of the major axes of the polarization ellipse in the plane (c.f.

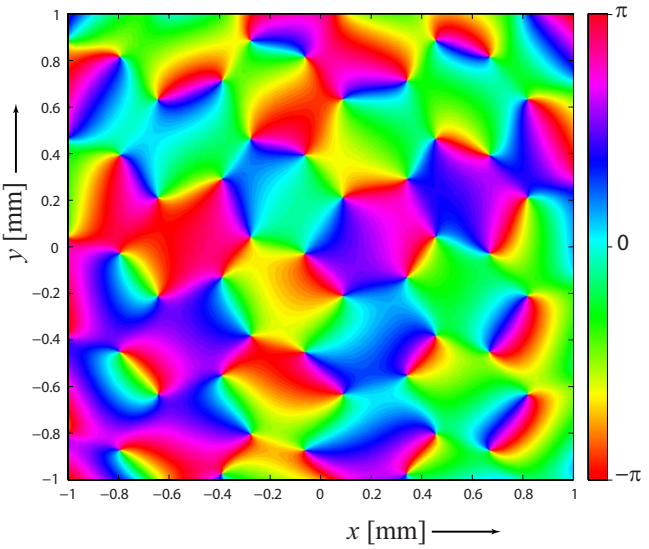

FIG. 6. (Color online) The phase of $\psi=\mathbf{E}\cdot\mathbf{E}$. All C points coincide with phase singularities of the quantity ψ. In this example $d=1$ mm and $\lambda=632.8$ nm.

Fig. 7 of [8]). For example, between the two vertical L lines located near $x=-0.7$ mm and $x=-0.4$ mm, the C point near $y=-0.9$ mm is a lemon, the one above it is a star, and they alternate as the vertical position increases.

An alternative way of locating C points is to plot the phase of the quantity $\psi=\mathbf{E}(\mathbf{r},\omega)\cdot\mathbf{E}(\mathbf{r},\omega)$ [3]. This is done in Fig. 6. The advantage of this approach is that both left-handed and right-handed C points are now simultaneously visible as phase singularities of ψ. These singularities have a charge that is twice the C-point charge, with the sign of the charge being indicative of the handedness of the polarization.

The symmetry in the three-pinhole arrangement as presented above is not necessary to create such a rich topology of singular structures. As an example of a configuration where the pinhole locations are not symmetric, we consider the case where

$$\mathbf{r}_1 = d(0.8,1,0), \quad \mathbf{r}_2 = d(1,0,0), \quad \mathbf{r}_3 = d(0,0,0) \tag{36}$$

and

$$\hat{\mathbf{e}}_1 = (0,1,0), \quad \hat{\mathbf{e}}_2 = (0.8,-0.6,0), \quad \hat{\mathbf{e}}_3 = \left(\frac{\sqrt{3}}{2},\frac{-1}{2},0\right). \tag{37}$$

Again, the field at each pinhole is taken to be of equal amplitude and co-phasal, and so Eq. (22) still applies. In Fig. 7, the spectral density of the field is shown in the plane $z=1$ m. The V point (a point of zero spectral density) has disappeared. Also, the pattern of L lines is changed as compared to the symmetric case, with the lines no longer crossing each other. In Fig. 8, the phases of $E_+(\mathbf{r},\omega)$ and $E_-(\mathbf{r},\omega)$ are shown. Breaking the symmetry in pinhole locations changes the number of C points and L lines in a region, but it does not result in their disappearance. The occurrence of L lines and C points may therefore be said to be generic. Note that the two figures are no longer mirror images of one another—the location of a phase singularity of $E_+(\mathbf{r},\omega)$ is no longer indicative of a location of a phase singularity of $E_-(\mathbf{r},\omega)$. It is seen that linear polarization and both types of circular polarization can all occur in the vicinity of points of near-zero spectral density.

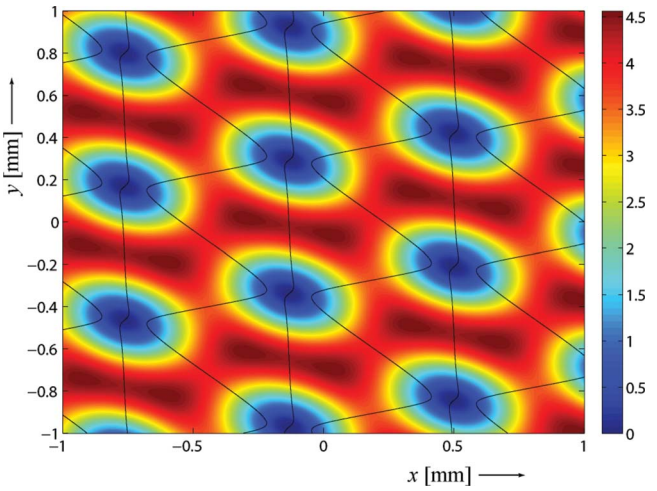

FIG. 7. (Color online) The spectral density in the $z=1$ m plane for an asymmetric three-pinhole experiment. The solid black curves are lines of linear polarization. In this example $d=1$ mm and $\lambda=632.8$ nm.

IV. *N*-PINHOLE INTERFEROMETER

Young's experiment can be easily generalized from Eqs. (3) and (22) by changing the bound on the summation to N. The number of free parameters (e.g., the state of polarization of the electric field at each pinhole, and the location of the pinholes) make any absolute statement about the scalability of the previous analysis impossible. However, if the phase and amplitude of the field at each pinhole are the same, and the direction of linear polarization and the location of the pinholes are radially symmetric, a pattern does emerge. The V line $x=0$, $y=0$ is present for all $N\geq 3$. In any transverse observation plane, an N-fold symmetry exists in the location of L lines and C points. This is illustrated in Fig. 9 where plots of S_0 and the phase of $E_-(\mathbf{r},\omega)$ are shown for the cases $N=4$ and $N=7$. The phase of $E_+(\mathbf{r},\omega)$ can be inferred from the phase of E_- through symmetry considerations.

V. CONCLUSION

We have studied the superposition of N linearly polarized fields in an N-pinhole interferometer. Despite the absence of

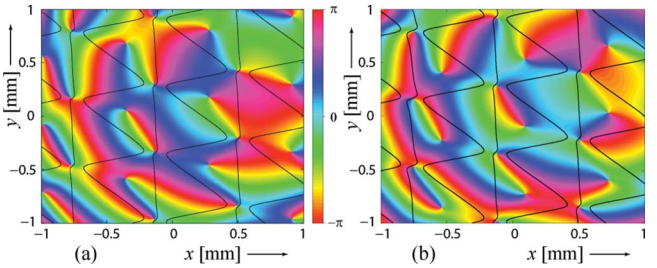

FIG. 8. (Color online) The phase of (a) $E_-(\mathbf{r},\omega)$, and the phase of (b) $E_+(\mathbf{r},\omega)$ in the $z=1$ m plane for an asymmetric three-pinhole configuration with $d=1$ mm and $\lambda=632.8$ nm.

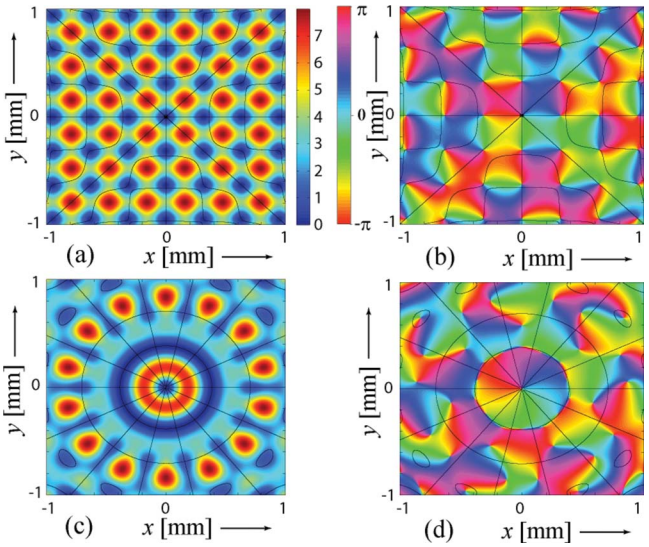

FIG. 9. (Color online) (a) The spectral density and (b) the phase of $E_{-}(\mathbf{r},\omega)$ for the four-pinhole case, and for the seven-pinhole case [(c) and (d)], both in the $z=1$ m plane with $d=1$ mm and $\lambda=632.8$ nm.

interference fringes when fields with two orthogonal polarization states are used, the two-pinhole case still yields an interesting structure of a finite number of semihyperboloids on which the state of polarization is linear. The three-pinhole interferometer gives a much richer topological behavior. *L* lines and *C* points were identified, and their occurrence was found to be generic. The generalization to an *N*-pinhole configuration was discussed for the case of a radially symmetric system.

ACKNOWLEDGMENTS

The authors thank an anonymous reviewer for helpful comments. R.W.S. acknowledges support by the Air Force Office of Scientific Research (Grant No. MURI F-49620-03-1-0379). T.D.V. was supported by the Foundation for Fundamental Research on Matter (FOM) and by the Dutch Technology Foundation (STW).

APPENDIX: DEGENERACY OF LINEAR POLARIZATION STATES FOR THE TWO-PINHOLE INTERFEROMETER

Any choice for the direction of linear polarization of the electric field at the two pinholes may, without loss of generality, be described as

$$\hat{\mathbf{e}}_1 = \hat{\mathbf{x}}, \quad \hat{\mathbf{e}}_2 = \cos\alpha\hat{\mathbf{x}} + \sin\alpha\hat{\mathbf{y}}. \tag{A1}$$

On substitution in Eqs. (3) and (10), and imposing the condition for linear polarization (i.e., $S_3=0$), we obtain the expression

$$\sin\alpha\,\sin[k(R_2-R_1)] = 0. \tag{A2}$$

This condition can be satisfied when $\alpha=0$, which is the trivial case in which the field at both pinholes is *x* polarized. The second solution, $k(R_2-R_1)=m\pi$, with *n* an integer, is identical to Eq. (11), and results in surfaces of linear polarization. Note that relaxing the condition that the field in each pinhole is co-phasal with each other changes the condition for linear polarization to $kR_1-kR_2=n\pi+\beta$, where β is the relative phase. This equation still yields a collection of hyperboloids, although the plane at $x=0$ is now no longer an *L* surface.

For circular polarization to occur, the field must satisfy $E_x(\mathbf{r},\omega)=\pm iE_y(\mathbf{r},\omega)$. Again using Eq. (A1), a simple calculation yields the conditions $R_1=R_2$ and $\alpha=\pi$. These two conditions actually result in $\mathbf{E}=\mathbf{0}$ on the plane $x=0$. A surface of circular polarization can be created by relaxing the condition that the field in each pinhole is of equal amplitude. Instead, if the field amplitudes in the two pinholes have a ratio $|E_x|/|E_y|=\gamma$ such that γ simultaneously solves $R_1=\gamma R_2$ and $(\gamma-1)kR_2=(2n+1)\pi/2$ for some integer *n* at a point $\mathbf{r}$, then the conditions for circular polarization can be met on, at most, a single hyperboloid.

[1] J. F. Nye, *Natural Focusing and Fine Structure of Light* (IOP, Bristol, 1999).
[2] M. S. Soskin and M. V. Vasnetsov, in *Progress in Optics*, edited by E. Wolf (Elsevier, Amsterdam, 2001), Vol. 42.
[3] M. V. Berry and M. R. Dennis, Proc. R. Soc. London, Ser. A **457**, 141 (2001).
[4] M. R. Dennis, Opt. Commun. **213**, 201 (2002).
[5] I. Freund, A. I. Mokhun, M. S. Soskin, O. V. Angelsky, and I. I. Mokhun, Opt. Lett. **27**, 545 (2002).
[6] A. I. Mokhun, M. S. Soskin, and I. Freund, Opt. Lett. **27**, 995 (2002).
[7] M. S. Soskin, V. Denisenko, and I. Freund, Opt. Lett. **28**, 1475 (2003).
[8] R. W. Schoonover and T. D. Visser, Opt. Express **14**, 5733 (2006).
[9] G. Gbur, T. D. Visser, and E. Wolf, Phys. Rev. Lett. **88**, 013901 (2001).
[10] D. G. Fischer and T. D. Visser, J. Opt. Soc. Am. A Opt. Image Sci. Vis. **21**, 2097 (2004).
[11] D. M. Palacios, I. D. Maleev, A. S. Marathay, and G. A. Swartzlander, Jr., Phys. Rev. Lett. **92**, 143905 (2004).
[12] G. A. Swartzlander, Jr. and J. Schmit, Phys. Rev. Lett. **93**, 093901 (2004).
[13] W. Wang, Z. Duan, S. G. Hanson, Y. Miyamoto, and M. Takeda, Phys. Rev. Lett. **96**, 073902 (2006).
[14] I. D. Maleev and G. A. Swartzlander, Jr., J. Opt. Soc. Am. B **25**, 915 (2008).
[15] G. Gbur and G. A. Swartzlander, J. Opt. Soc. Am. B **25**, 1422 (2008).
[16] H. F. Schouten, G. Gbur, T. D. Visser, and E. Wolf, Opt. Lett. **28**, 968 (2003).
[17] G. Gbur, T. D. Visser, and E. Wolf, Opt. Commun. **239**, 15

(2004).
[18] C. H. Gan and G. Gbur, Opt. Commun. **280**, 249 (2007).
[19] L. Basano and P. Ottonello, Phys. Rev. Lett. **94**, 173901 (2005).
[20] D. Ambrosini, F. Gori, and D. Paoletti, Opt. Commun. **254**, 30 (2005).
[21] G. Ruben and D. M. Paganin, Phys. Rev. E **75**, 066613 (2007).
[22] T. D. Visser and R. W. Schoonover, Opt. Commun. **281**, 1 (2008).
[23] R. Loudon, *The Quantum Theory of Light*, 3rd ed. (Oxford University Press, Oxford, 2000).
[24] C. Brosseau, *Fundamentals of Polarized Light* (Wiley, New York, 1998).
[25] B. J. Davis and P. S. Carney, J. Opt. Soc. Am. A Opt. Image Sci. Vis. **25**, 2102 (2008).
[26] M. Born and E. Wolf, *Principles of Optics: Electromagnetic Theory of Propagation, Interference and Diffraction of Light*, 7th ed. (Cambridge University Press, Cambridge, 1999).
[27] K. S. Youngworth and T. G. Brown, Opt. Express **7**, 77 (2000).
[28] J. D. Jackson, *Classical Electrodynamics*, 3rd ed. (Wiley, New York, 1998).
[29] M. R. Dennis, Opt. Lett. **33**, 2572 (2008).